















Continuous spatial self-cleaning in GRIN multimode fiber for self-referenced multiplex CARS imaging

S. WEHBI,^{1,2} T. MANSURYAN,^{2,*}  K. KRUPA,³  M. FABERT,² 
A. TONELLO,²  M. ZITELLI,⁴  M. FERRARO,⁴  F. MANGINI,^{4,5} 
Y. SUN,⁴  S. VERGNOLE,¹  H. KANO,⁶  S. WABNITZ,⁴ 
AND V. COUDERC² 

¹ALPhANOV, Optics & Lasers Technology Center, Institut d'optique d'Aquitaine, Rue François Mitterrand, 33 400 Talence, France

²Université de Limoges, XLIM, UMR CNRS 7252, 123 Av. A. Thomas, 87060 Limoges, France

³Institute of Physical Chemistry, Polish Academy of Sciences, Warsaw, ul. Kasprzaka 44/52, 01-224, Poland

⁴Dipartimento di Ingegneria dell'Informazione, Elettronica e Telecomunicazioni, Sapienza University of Rome, Via Eudossiana 18, 00184 Rome, Italy

⁵Department of Information Engineering, University of Brescia, Via Branze 38, 25123 Brescia, Italy

⁶Department of Chemistry, Faculty of Science, Kyushu University, 744 Moto-oka, Nishi-ku, Fukuoka 819-0395, Japan

*tigran.mansuryan@xlim.fr

Abstract: We demonstrate how spatial beam self-cleaning and supercontinuum generation in graded-index multimode optical fibers can be directly applied in multiplex coherent anti-Stokes Raman Scattering (M-CARS) spectroscopy. Although supercontinuum generation causes pump depletion mainly in the center of the beam, the partial recovery of the pump brightness due to self-cleaning may enable self-referenced M-CARS, with no additional delay lines to synchronize pump and Stokes waves. As a proof-of-principle, we report examples of imaging of single chemical compounds and polystyrene beads. The new scheme paves the way towards simpler M-CARS systems based on multimode fiber sources.

© 2022 Optica Publishing Group under the terms of the [Optica Open Access Publishing Agreement](#)

1. Introduction

Coherent Anti-Stokes Raman Scattering (CARS) is a well-known process, largely studied in the past since the pioneering work of P. D. Maker and R. W. Terhune in 1965 [1], and further developed in 1974 by R. F. Begley et al. [2]. This nonlinear four-wave mixing (FWM) process, involving molecular vibrational modes, has been later used in a non-collinear geometry for studying pure organic liquids and deuterated water in onion-skin cells [3]. In 1982, Zumbusch *et al.* used CARS microscopy in a forward collinear configuration, to measure the vibrational signature of the CH region in the spectral range between 2800 cm^{-1} and 3200 cm^{-1} [4]. A multiplex CARS (M-CARS) experiment has been carried out in 2002, by using a combination of both wide-band and narrow-band laser sources [5–7].

In this context, the advent of microstructured nonlinear optical fibers [8] has allowed for the generation of wide-band supercontinuum (SC) with low input pump pulse energies. SC generation by means of femtosecond laser pulses [9], and its application to high spectral resolution M-CARS have already been demonstrated [11–13]. However, in femtosecond-based SC, the group velocity dispersion of optical fibers severely reduces the temporal overlap between pump and Stokes waves in CARS: as a result, the time delays of Stokes and pump wave-packets should be carefully synchronized. To overcome this limit, longer pulses (up to a few nanoseconds) have

been used [10–13]. Microchip laser sources delivering pulses of several hundreds of picoseconds (~600 ps) permit to generate stable SC for nonlinear imaging [14]. However, even these light sources are not directly suitable for M-CARS spectroscopy. In fact, in silica fibers the spectral broadening introduced by $\chi^{(3)}$ nonlinearities, such as the instantaneous Kerr effect and the delayed Raman response, seriously depletes sub-nanosecond pump pulses. The remaining pump power is mainly located in time slots at the leading and trailing edges of the pump pulse, which are a few hundreds of picoseconds far apart with respect to the SC [15]. Unfortunately, this fact prevents any further nonlinear mixing, owing to the lack of temporal overlap between the residual pump and the SC. The problem can be solved by adding an intact pump through an additional delay line, for temporally synchronizing the pump with the large-band Stokes waves [11–14].

Over the past few years, multimode optical fibers (MMF) have received a renewed interest, thanks to the possibility of generating coherent light sources, which are suitable for key applications such as nonlinear imaging and multispectral LIDAR. In this framework, a nonlinear effect called spatial beam self-cleaning was demonstrated in graded index (GRIN) MMFs, by using laser pulses with durations ranging from femtoseconds up to sub-nanoseconds [16–19]. Self-cleaning is based on the action of many spatial intermodal FWM processes, that are phase-matched by means of a periodic index grating created by the Kerr effect, and by the equal spacing of modal wave vectors in GRIN MMFs [20]. A non-reciprocal nonlinear phase effect, which accompanies the many-mode nonlinear coupling, induces an energy redistribution with a net flow toward the fundamental mode, and a partial redistribution towards higher-order-modes (HOM). As a result, a quasi-single mode emission, superimposed on a background of weak intensity, can be obtained at the output of a GRIN MMF. Interestingly, spatial beam self-cleaning is very robust against fiber handling and bending [19]. In the time domain, the coherent pulse compression, which is observed in several experiments, proves the spatiotemporal nature of this effect: the combined action of spatial and temporal reshaping increases the output peak power, and consequently the beam brightness, with respect to the case of quasi-linear propagation [21]. The nonlinear self-cleaning effect occurs spontaneously in GRIN MMFs, and it has been already explored for SC generation [22,23], optical poling for second-harmonic generation [24,25] and more recently also for multiphoton fluorescence imaging [26]. Its physical mechanism has been discussed in the framework of thermodynamic and wave turbulence approaches, providing interesting insights into the subject [27–30].

In this paper, we demonstrate that spatial beam self-cleaning obtained in GRIN MMFs can also provide a suitable, ready-to-use light source for M-CARS applications. In particular, by using GRIN MMFs it is possible to get rid of delay lines, thus significantly simplifying the CARS imaging set-up. In this work, we show that a direct mixing between the SC and the remaining pump beam is possible. Our interpretation of the obtained results is the coexistence of additional energy flows. The first flow is the SC generation, which dominantly depletes the center of the pump, in order to create new spectral components. At the same time, the pump brightness is constantly recovered by the self-cleaning process, thanks to the energy stored in HOMs, and continuously flowing toward the fundamental mode. Overall, the combination of the SC and residual pump light turns out to be suitable for obtaining M-CARS spectra. In order to confirm this point, we obtained M-CARS spectra and imaging of simple compounds, such as polystyrene beads.

2. Experimental set-up

The experimental setup is sketched in Fig. 1. It is composed of a fiber laser emitting 300 fs pulses at 1030 nm with an adjustable repetition rate between 0 and 2 MHz. The pulses are then stretched to 100 ps, in order to generate efficient SC and to avoid a walk-off between pump and Stokes wavelengths in the fiber. The laser beam power and polarization state are controlled by means of a half-wave plate and a polarizer. A convergent lens with 50 mm of focal length is used to couple

the infrared light into the optical fiber. We used a GRIN MMF with a core diameter of $52.1\ \mu\text{m}$ and a numerical aperture of 0.205. We considered two different fiber lengths of 30 m and 13 m, respectively. The beam diameter at the fiber input is $30\ \mu\text{m}$ at full-width-at-half-maximum (FWHM) of intensity: this choice allows for exciting ~ 100 guided modes at normal incidence. The beam at the fiber output is collimated by means of a convergent lens ($f = 30\ \text{mm}$). Three different optical filters are used to shape the SC spectrum. F1 is a Thorlabs FELH1000 longpass filter (cut-on wavelength: 1000 nm), which was used to remove the visible-NIR up to 1000 nm, as this radiation would spoil the CARS signal. Thorlabs NF1064 notch filter (F2) has a 44 nm FWHM, which permits us to isolate the pump wavelength from the Stokes wavelengths. The last Semrock LP02-1064RE longpass filter (F3) has a cut-on wavelength at 1064 nm. This cut-on value can be varied toward the pump (1030 nm), by choosing an appropriate incidence angle. Thus, the combination of filters F2 and F3, with a fine-tuning of their angles, permits us to carve the Stokes spectrum, and to isolate a narrow bandwidth around the pump (Fig. 2(d)). Such a combination of optical filters can significantly improve the M-CARS spectral resolution. The spectrally reshaped beam is then sent to the Nikon scanning stage microscope, operating in a forward confocal configuration. Two microscope objectives Obj1 (Olympus LUMFLN60XW) and Obj2 (Nikon S Plan Fluor ELWD 60x) are used to focus light on the sample, and to collect the CARS signal, respectively. All of the light emitted by the sample is sent to the Horiba LabRAM Raman spectrometer for CARS spectral measurements, and for the related image reconstruction of the sample.

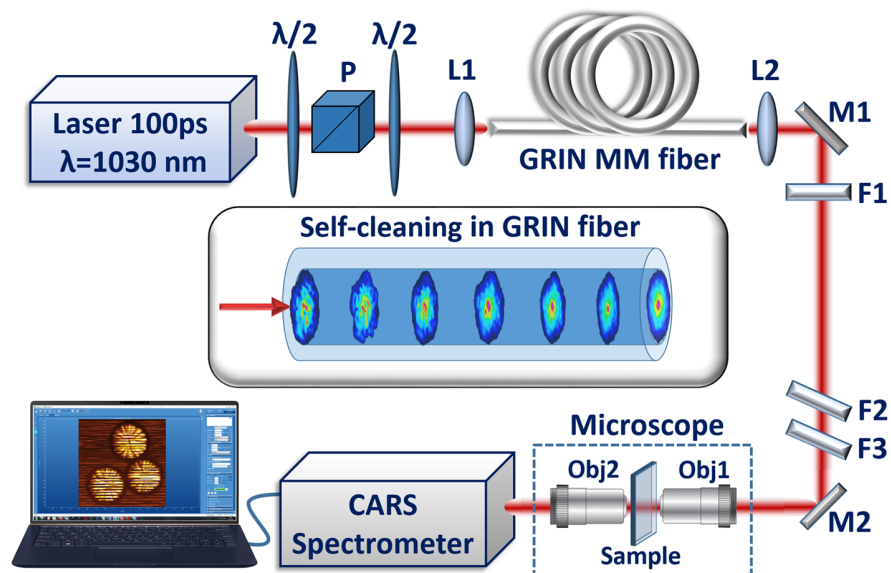


Fig. 1. Set-up of M-CARS experiment with GRIN multimode fiber. $\lambda/2$, half-wave plate; P, polarizing cube; L1, L2, coupling and collimating lenses; MM, multimode; M1, M2, mirrors; F1, F2, F3, optical filters; Obj1, Obj2, microscope objectives. Sample is fixed on the scanning stage. Inset shows an example of spatial self-cleaning process in GRIN fiber.

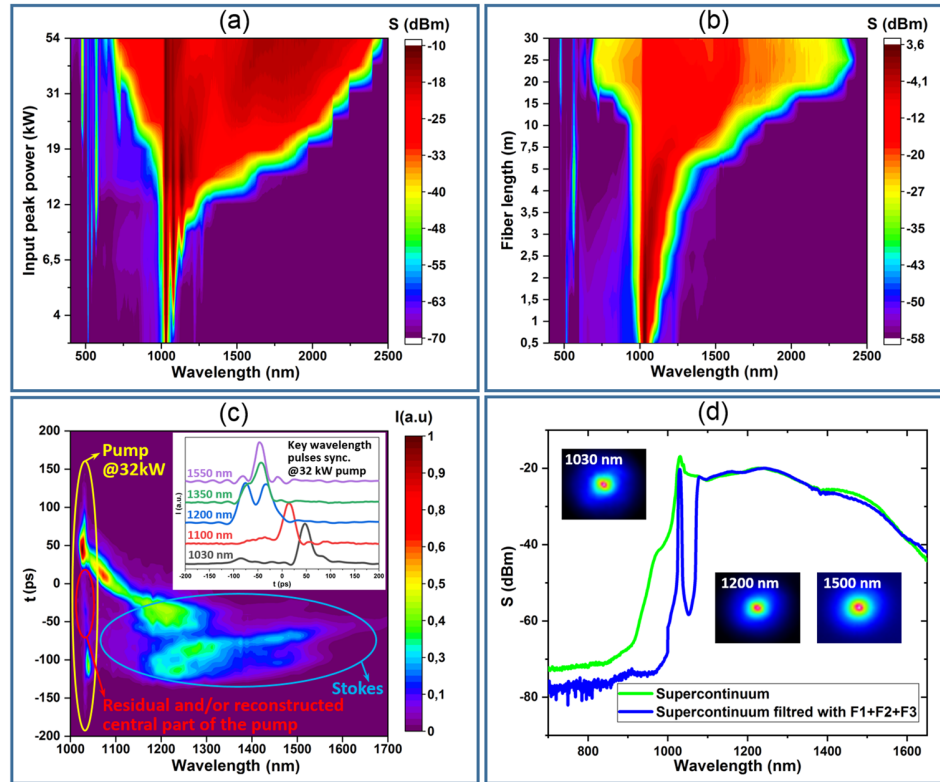


Fig. 2. Spectral evolution in our system. (a) SC generation in 30-m-long GRIN MMF vs. input pump peak power (P_c); (b) SC generation vs. fiber length at $P_c = 45$ kW; (c) Spectrogram measured at $P_c = 32$ kW for a fiber length $L_{\text{Fibre}} = 13$ m clearly, which shows the temporal delay between different spectral components of the output beam. Inset highlights the temporal overlap between pump pulse and several other wavelengths; (d) SC right after the fiber (green trace) and after spectral filtering with long-pass and notch filters (blue trace), before sending the light into the microscope. Insets show the quasi-Gaussian profile of the output beam at the typical wavelengths that are involved in the CARS interaction.

3. Spatial self-cleaning and supercontinuum generation

In a first step, we analyzed the self-cleaning process, which is obtained in the GRIN MMF at the pump wavelength, as illustrated in the inset of Fig. 1. Self-cleaning of the output beam profile occurs when the input power overcomes a certain threshold, which is estimated to be around 1.5 kW in our system. For input powers above such a threshold, the speckled output pattern progressively evolves into a quasi-single-mode beam. Several implementations of the spatial self-cleaning can be found, for instance, in Refs. [18–21].

In a second step, we analyzed the spectral broadening that follows the self-cleaning. When the input power grows larger than the threshold for self-cleaning, stimulated Raman scattering comes into play, generating three Stokes sidebands in a spectral range up to 1.3 μm . By further increasing the pump power, and for wavelengths propagating in the anomalous dispersion regime, (that is above 1.3 μm), modulation instability leads to soliton generation. Then, activated by the Raman gain, soliton self-frequency shift occurs, which leads to SC generation up to 2.4 μm , as illustrated in Fig. 2(a). At the same time, the Raman Stokes peaks are progressively smoothed

because of Raman gain saturation. Thus, spectral broadening is mainly generated in the infrared domain, with only weak spectral conversion in the range between 700 nm and 1030 nm, because of dispersive wave generation [22,23]. The maximum spectral broadening, which is obtained for a 30-m long fiber at 55 kW of input power (fiber end-face damage threshold), spans from 700 nm to 2400 nm (Fig. 2(a)). By managing the polarization state orientation of the input pump, we could also minimize the geometric parametric instability (GPI) sidebands that appear in the visible domain, so that they are not visible in the experiments of Fig. 2. Moreover, we carefully investigated the evolution of spectral broadening by fiber cutback measurements at a pump peak power of 45 kW (Fig. 2(b)). This analysis helped us to identify the best suitable fiber length (about 13 m) that is needed to generate large-band Stokes waves ranging from 0 to 4000 cm^{-1} (that is, from 1030 nm up to 1750 nm for a pump at 1030 nm).

In a third step, we measured the spectro-temporal dynamics of the SC, which was generated with the optimal fiber length of 13 m (Fig. 2(c)). We carried out this analysis by direct detection, and using a photodiode of 45 GHz, connected to the fast oscilloscope with 70 GHz of bandwidth. The resulting spectrogram allowed us to identify the range of SC wavelengths whose associated temporal profiles still overlap with the pump. From Fig. 2(c) we can see that, although the pump pulse is largely depleted, a weak residual pump portion remains between 0 and -100 ps, which is synchronized in time with the entire supercontinuum spectrum. This is more evident in the inset of Fig. 2(c) inset, where the temporal overlap among some key wavelengths is presented.

For nanosecond pulses, there is no appreciable temporal shift between the SC and the depleted central part of the pump pulse. In the present case, with 100 ps pulses, we noticed the presence of a small time shift due to temporal walk-off, as it can be seen in Fig. 2(c).

In our M-CARS measurements we used the SC generated from 13 m of GRIN MMF (green trace in Fig. 2(d)). The spectrum sent to the microscope was then composed by a sharp line at 1030 nm, provided by the output pump wave (with bandwidth of 4 nm), and a SC ranging from 1075 nm to 1700 nm, that was used for M-CARS (blue trace in Fig. 2(d)). Note that the spectral dip, separating the pump line and the SC, is about 40 nm wide and has more than 40 dB of depth. Moreover, all wavelengths between $1\text{ }\mu\text{m}$ and $1.7\text{ }\mu\text{m}$ are carried by bell-shaped beams (see insets of Fig. 2(d)).

4. Temporal synchronization from spatial self-cleaning

In our setup, the spatial self-cleaning process plays a crucial role. This process is first obtained at the pump wavelength, in the absence of any frequency conversion [19]. SC in the GRIN fiber is mainly carried by the fundamental mode, and its generation efficiency is boosted by spatiotemporal dynamics. Although SC generation leads to a drastic depletion of the top portion of pump pulses, in the presence of spatial self-cleaning one may expect the occurrence of nonlinear mode redistribution of the pump beam. As a result, the pump energy, which is initially carried by HOMs, continuously refills the fundamental mode. In this perspective, spatial self-cleaning allows to “refresh” the pump beam along its propagation in the fiber, which in turn may facilitate M-CARS interactions within the entire spectral range of the Stokes or SC beam. In fact, all along the process of self-cleaning the beam remains multimode, due to the presence of two energy flows: a direct cascade towards the HOMs and an inverse cascade towards the fundamental mode. The dynamics related to the presence of these two energy flows were discussed in [27–30]. It is then rather unlikely that, at some point in the fiber, all of the beam energy will be stored entirely in the fundamental mode. Using a slightly multimode pump has the consequence of reducing the M-CARS spatial resolution. However, this is largely compensated by the fact that the Stokes wave is mainly carried by the fundamental mode of the fiber, whose diameter determines the ultimate spatial resolution of our nonlinear imaging system.

We performed a series of numerical simulations, in order to confirm the experimental observations, and to obtain a deeper understanding of the pump feeding process during its

propagation in the MMF. The simulations refer to the case of a simplified scalar propagation of optical beams in the GRIN fiber. The model includes diffraction, dispersion, waveguide contribution, Kerr and Raman effects. The fiber core has an elliptical shape. The disorder, which leads to speckle formation as a result of beam propagation, is simulated by applying every 10 mm random deformations to the core shape. Specifically, the elliptical shape of the core is rotated by a sequence of random angles, varying between 0 and 2π rad. Each of the ellipse axes has a length that randomly fluctuates (obeying a uniform distribution) around the value of the fiber core diameter (with a maximum excursion of $0.2 \mu\text{m}$). In Fig. 3 we show the results of the numerical simulation for a GRIN fiber with a core diameter of $50 \mu\text{m}$. We used an input beam diameter of $30 \mu\text{m}$ at FWHM, a pump wavelength of 1064 nm , and an input peak intensity of $60 \text{ GW}/\text{cm}^2$; the input pulse duration was of 300 fs , and it was stretched to 12 ps before propagation in the GRIN fiber. The propagation length was limited to 0.8 m , in order to reduce the computational time. Figure 3(a) shows the output temporal pulse envelope (dB scale), obtained with an optical filter of 300 GHz bandwidth applied at different central wavelengths. It is worth studying the spatial dependence of the M-CARS expected efficiency as a function of the transverse position of the beam (say, the x coordinate, for a fixed y value at the fiber center). M-CARS will be active whenever pump and Stokes signals are temporally (and spatially) superimposed.

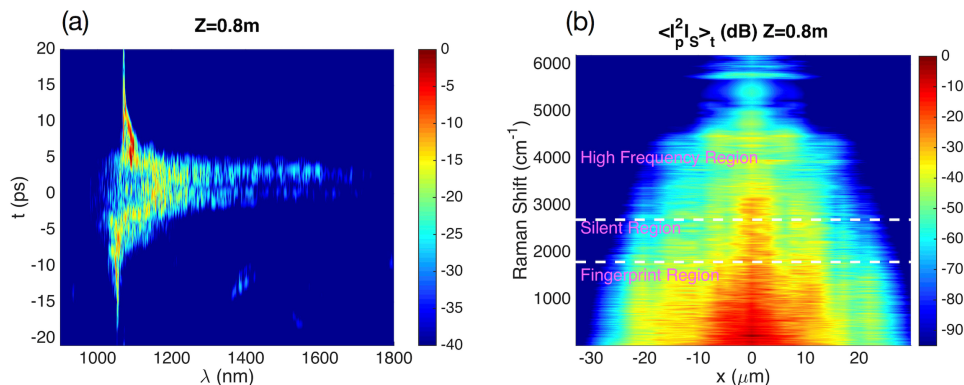


Fig. 3. Numerically calculated SC generation in a 0.8 m long multimode GRIN fiber of $50 \mu\text{m}$ core. (a) Pulse envelopes in the time domain, obtained by applying a 300 GHz filter at different central wavelengths (dB scale). (b) Corresponding spectro-spatial distribution of the potential M-CARS signal averaged in time.

The higher the value of $I_p^2 I_s$, being I_p , I_s , the pump and Stokes intensities, respectively, the easier is to detect the resonance with M-CARS. One would expect that the CARS signal is mainly detected on-axis, because the SC has higher intensity for low-order modes (owing to the spatial self-cleaning process). Figure 3(b) illustrates the evolution of the time average of the product $\langle I_p^2 I_s \rangle_t$. We can see how the signal $\langle I_p^2 I_s \rangle_t$ has the maximum intensity at the center of the core. Thus, we may argue that the same will happen for the M-CARS signal. However, it is important to remind that, while Fig. 3(b) is simply calculated starting from the output near-field filtered at the two relevant central wavelengths of the pump and Stokes beams, the experimental M-CARS signal is instead measured after the beam is focalized in the sample by a microscope objective. We may also notice from Fig. 3(b) that the spectral broadening is large enough to cover both the fingerprint region (from 400 cm^{-1} to 1800 cm^{-1}) and silent region (from 1800 cm^{-1} to 2700 cm^{-1}).

To complete our study, we also considered in the numerical simulations a slightly different configuration: the corresponding results are reported in Fig. 4. In this second case, we assumed

a peak intensity of 40 GW/cm^2 , the input beam diameter of $20 \mu\text{m}$, and the pulse was transform-limited with a temporal duration of 16 ps . Figure 4(a) illustrates the evolution of the signal $I_p^2 I_s$ upon time and wavenumber shift: from these results, one expects a maximum M-CARS efficiency to happen close to the pulse peak power value. At the same time, Fig. 4(b) illustrates the corresponding spatial dependence upon the transverse coordinate x of $\langle I_p^2 I_s \rangle_t$. From these figures, we can expect that in this case the M-CARS signal is gainful in the fingerprint region as well as in the *high frequencies* (HF, from 2700 cm^{-1} to 4000 cm^{-1}) region: this enhancement can be ascribed to the action of GPI. On the other hand, a minimum of the signal appears in the silent region. This particularity can be associated with the choice of the fiber type, since the generation of GPI sidebands is directly influenced by fiber parameters, such as the fiber core diameter and the refractive index difference. In this second case, the silent region cannot be efficiently explored, due to the expected low level of M-CARS signal that one can obtain. Such a gap can be possibly filled in practice by increasing the peak power, or by adjusting the orientation of the initial state of polarization of the pump.

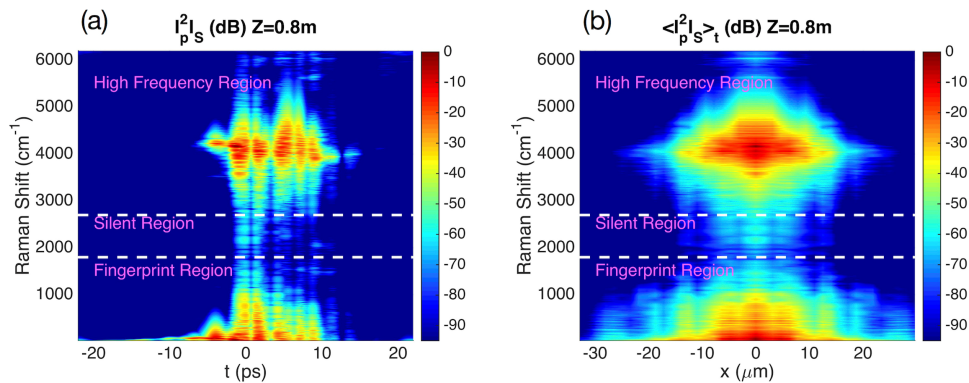


Fig. 4. Numerically calculated SC generation in a 0.8 m long multimode GRIN fiber with a code diameter of $65 \mu\text{m}$. (a) spectro-temporal distribution of the potential M-CARS signal (dB scale). (b) Corresponding spectro-spatial distribution of the potential M-CARS intensity.

5. M-CARS experiment

With the previously described setup, we performed M-CARS measurements by launching the spectrally reshaped SC into a microscope-spectrometer system in confocal imaging configuration. First, we performed the measurements of chemical samples such as methanol, acetone and paraffin. The raw M-CARS spectra are displayed in Fig. 5.

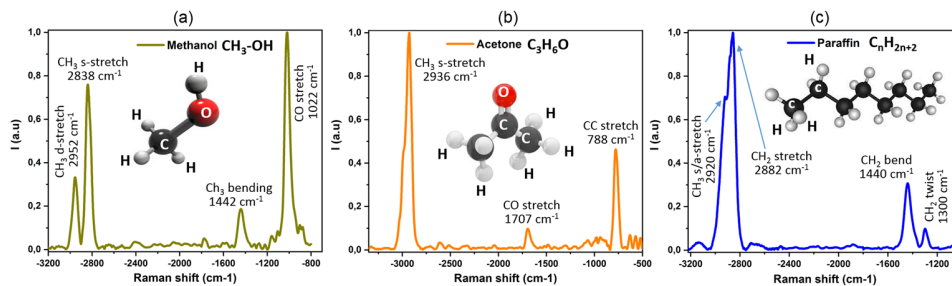


Fig. 5. M-CARS spectrum of (a) methanol, (b) acetone, and (c) paraffin.

The spectral resolution was estimated to be of 40 cm^{-1} (which corresponds to the 4 nm bandwidth of our pump), being directly dependent on the spectral filtering of the pump wave, as discussed above. We found a good agreement between the spectra measured with our set-up, and those reported in the literature, since the main vibrational signatures of each chemical element were retrieved. For methanol molecules, the spectrum is composed of the lines at 2952 cm^{-1} , 2838 cm^{-1} , 1442 cm^{-1} and 1022 cm^{-1} that are due to the CH_3 d-stretching, CH_3 s-stretching, CH_3 bending and CO stretching modes, respectively [31]. The CH_2 stretching at 2936 cm^{-1} , the CO stretching at 1707 cm^{-1} and the CC stretching at 788 cm^{-1} have been identified for acetone [31]. The paraffin sample has been characterized instead by identification of the lines at 2920 cm^{-1} , 2882 cm^{-1} , 1440 cm^{-1} , and 1300 cm^{-1} , corresponding to the CH_3 stretching, the CH_2 stretching, the CH_2 bending and the CH_2 twisting modes, respectively [32].

Finally, we analyzed a sample of polystyrene beads, as illustrated in Fig. 6. The beads are $20\text{ }\mu\text{m}$ in diameter, and with characteristic $0.5\text{ }\mu\text{m}$ wide cracks (brightfield microscope image of beads shown in Fig. 6(a)). The cracks are due to the mechanical stress of mounting, between the microscope slide and the coverslip. The sample, which consists of two beads, was fixed on the scanning stage of our microscope, and examined by $0.5\text{ }\mu\text{m}$ scanning step. The M-CARS spectrum of each pixel was registered with the LabRAM spectrometer (green traces in Fig. 6(b)). We properly filtered (color spectral window in Fig. 6(b)) the obtained spectra, in order to select only the vibrational signature at 1002 cm^{-1} that corresponds to the breathing mode of the aromatic carbon ring of polystyrene. The intensity level at this vibrational frequency was used to construct the M-CARS image (Fig. 6(c)). In this case, we obtained an M-CARS image with an estimated spatial resolution of $1\text{ }\mu\text{m}$. The pixel integration time was of 0.5 s ; the horizontal stripes of Fig. 6(c) are caused by the recurrent action of the laser power stabilizer.

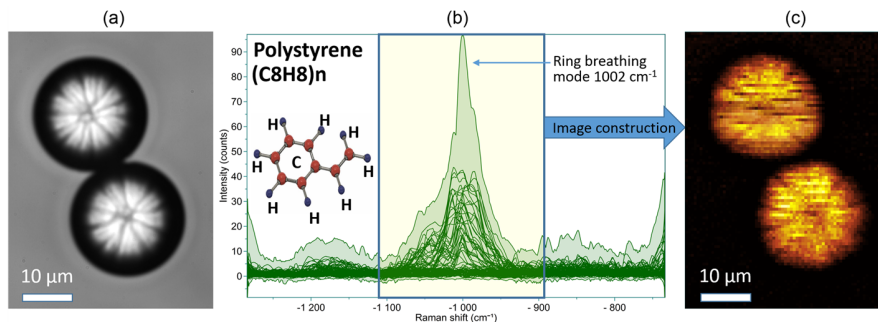


Fig. 6. (a) Linear brightfield image of the polystyrene beads; (b) M-CARS spectra of polystyrene beads between 1300 cm^{-1} and 750 cm^{-1} ; (c) M-CARS image of the polystyrene beads at 1002 cm^{-1} .

6. Discussion

As discussed in section 3, in our experiments the maximum power was limited by the damage threshold of the GRIN fiber. One can increase such a threshold by using a pure silica fiber end cap. The spatial resolutions obtained in the current experiments are close to the diffraction limit at the selected wavelengths, and they are also comparable to the values reported in Ref. [26]. It should be pointed out that the spectral power scales used in both numerical simulations and in the experiments (Fig. 2) are given in arbitrary units, and they do not represent the actual power values.

We believe that our source has comparable performances with those of existing well-known M-CARS systems. Our first tests have been done on liquid samples: methanol, paraffin, acetone

(Fig. 4). For dimmer samples, it would be necessary to increase either the spectrometer integration time or the excitation power (by increasing the repetition rate of the laser, or the pump peak power in the fiber). Thickness control of biological samples is also very useful. In the case of poorly transparent samples, it could be possible to work in “epi” configuration.

At the output of the fiber, the SC average power was about 1 W at 300 kHz of laser repetition rate. Since the pump power as a whole was about 100 mW, we may estimate that its residual central part carries a power of about 5 mW. A weak pump could limit the CARS efficiency, but not in the way one would expect. Besides the proper CARS signal itself, there is always a large non-resonant background. The resonant to non-resonant ratio remains fixed, and it cannot be enhanced by increasing the laser pump power. Therefore, once identified that the power level is large enough to overcome the detector noise and to measure the non-resonant background, there is no need to increase the power any further. One can also increase the spectrometer integration time, if required. As for the residual pump to Stokes ratio, we see three possible ways to increase the pump power. First, we can increase the pump peak power by using a pure silica fiber end cap at the fiber input. Second, we can increase the average power by increasing the laser repetition rate. Finally, we can selectively amplify the pump only, at the output of the fiber, by using either a Yb:YAG (for 1030 nm) or a Nd:YAG (for 1064 nm) amplifier. Actually, the experiment with amplification at 1064 nm by using a Nd:YAG crystal was tested with success in our laboratory, but its results are not discussed here.

The experiments reported in the present work were carried out at 300 kHz. Since the repetition rate is adjustable in our laser, we have explored the impact of its variation. As a matter of fact, we obtained similar CARS results when varying the repetition rate from 15 kHz up to 2 MHz (not reported here). Obviously, accordingly to the repetition rate, one has to adjust the integration time of the spectrometer. In the literature, efficient CARS systems with light sources repetition rates ranging from 20 kHz to 80 MHz, and using femtosecond to nanosecond pulses, have been reported. In this perspective, our 100 ps 300 kHz system is in-line with state-of-the-art systems. We would like to stress that, besides to be self-referenced, the main advantage of our system is the multiplex method (M-CARS), which allows to simultaneously cover a range from 0 cm^{-1} to 5700 cm^{-1} (the frequency detuning from the pump of the whole SC up to 2500 nm; Fig. 2(a)). In particular, our system does not require any wavelength tuning-scanning, as it occurs in OPO systems.

7. Conclusion

We exploited the complex spatiotemporal dynamics of beam self-cleaning in multimode fibers to demonstrate a simplified, self-referenced M-CARS system based on the self-cleaning and spectral broadening of the input laser pulses. The continuous recovery of the fundamental mode by energy transfer from high-order modes, allowed for obtaining infrared SC generation with simultaneous preservation of the pump spectral component of the beam. Direct mixing between the SC and the remaining pump beam was demonstrated. Imaging and measurement of the M-CARS signature of several compounds was demonstrated. In particular, our system permits to cover simultaneously the range from 0 cm^{-1} to 5700 cm^{-1} . The spatial resolution was driven by the mutual superposition of the pump and the single-mode Stokes waves, and it is close to the diffraction limit. The spectral resolution can be reduced down to 40 cm^{-1} by properly adjusting the filters placed at the fiber end.

Present work opens the way for the development of new microscopic and endoscopic imaging systems by using multimode fibers.

Funding. Arianegroup (X-LAS); Direction Générale de l'Armement; Conseil Régional Aquitaine (F2MH, FLOWA, SI2P); Agence Nationale de la Recherche, (ANR-10-LABX-0074-01, ANR-15-IDEX-0003, ANR16-CE08-0031,

ANR-18-CEO80016-01); H2020 FET Open PETACom; H2020 European Research Council(740355, 874596); Narodowa Agencja Wymiany Akademickiej and French-Polish Partnership Hubert Curien, (POLONIUM program No° BPN/BFR/2021/1/00013, 48161TH).

Disclosures. The authors declare no conflicts of interest.

Data availability. Data underlying the results presented in this paper are not publicly available at this time but may be obtained from the authors upon reasonable request.

References

1. P. D. Maker and R. W. Terhune, "Study of Optical Effects Due to an Induced Polarization Third Order in the Electric Field Strength," *Phys. Rev.* **137**(3A), A801–A818 (1965).
2. R. F. Begley, A. B. Harvey, and R. L. Byer, "Coherent anti-Stokes Raman spectroscopy," *Appl. Phys. Lett.* **25**(7), 387–390 (1974).
3. M. D. Duncan, J. Reintjes, and T. J. Manuccia, "Scanning coherent anti-Stokes Raman microscope," *Opt. Lett.* **7**(8), 350 (1982).
4. A. Zumbusch, G. R. Holtom, and X. Sunney Xie, "Three-dimensional Vibrational Imaging by Coherent Anti-Stokes Raman Scattering," *Phys. Rev. Lett.* **82**(20), 4142–4145 (1999).
5. M. Müller and J. M. Schins, "Imaging the thermodynamic state of lipid membranes with multiplex CARS microscopy," *J. Phys. Chem. B* **106**(14), 3715–3723 (2002).
6. G. W. H. Wurpel, J. M. Schins, and M. Müller, "Chemical specificity in 3D imaging with multiplex CARS microscopy," *Opt. Lett.* **27**(13), 1093–1095 (2002).
7. X. Cheng, A. Volkmer, L. D. Book, and X. S. Xie, "Multiplex coherent anti-Stokes Raman scattering microspectroscopy and study of lipid vesicles," *J. Phys. Chem. B* **106**(34), 8493–8498 (2002).
8. J. C. Knight, T. A. Birks, P. S. J. Russell, and D. M. Atkin, "All-silica single mode optical fiber with photonic crystal cladding," *Opt. Lett.* **21**(19), 1547–1549 (1996).
9. J. K. Ranka, R. S. Windeler, and A. J. Stentz, "Visible continuum generation in air–silica microstructure optical fibers with anomalous dispersion at 800 nm," *Opt. Lett.* **25**(1), 25–27 (2000).
10. L. Provino, J. M. Dudley, H. Maillotte, N. Grossard, R. S. Windeler, and B. J. Eggleton, "Compact broadband continuum source based on a microchip laser pumped micro-structured fiber," *Electron. Lett.* **37**(9), 558–560 (2001).
11. M. Okuno, H. Kano, P. Leproux, V. Couderc, and H. Hamaguchi, "Ultrabroadband ($>2000\text{cm}^{-1}$) multiplex coherent anti-Stokes Raman scattering spectroscopy using a subnanosecond supercontinuum light source," *Opt. Lett.* **32**(20), 3050–3052 (2007).
12. M. Okuno, H. Kano, P. Leproux, V. Couderc, and H. Hamaguchi, "Ultrabroadband multiplex CARS microspectroscopy and imaging using a subnanosecond supercontinuum light source in the deep near infrared," *Opt. Lett.* **33**(9), 923–925 (2008).
13. M. Okuno, H. Kano, P. Leproux, V. Couderc, J. P. R. Day, M. Bonn, and H. Hamaguchi, "Quantitative CARS molecular fingerprinting of single living cells with the use of the maximum entropy method," *Angew. Chem. Int. Ed.* **122**(38), 6925–6929 (2010).
14. H. Segawa, M. Okuno, P. Leproux, V. Couderc, T. Ozawa, and H. Kano, "Multimodal imaging of living cells with multiplex coherent anti-Stokes Raman scattering (CARS), third-order sum frequency generation (TSFG) and two-photon excitation fluorescence (TPEF) using a nanosecond white-light laser source," *Anal. Sci.* **31**(4), 299–305 (2015).
15. A. De Angelis, A. Labrüyère, V. Couderc, P. Leproux, A. Tonello, H. Segawa, M. Okuno, H. Kano, D. Arnaud-Cormos, P. Lévêque, and H. Hamaguchi, "Time-frequency resolved analysis of a nanosecond supercontinuum source dedicated to multiplex CARS application," *Opt. Express* **20**(28), 29705–29716 (2012).
16. Z. Liu, L. G. Wright, D. N. Christodoulides, and F. W. Wise, "Kerr self-cleaning of femtosecond-pulsed beams in graded-index multimode fiber," *Opt. Lett.* **41**(16), 3675–3678 (2016).
17. W. H. Renninger and F. W. Wise, "Optical solitons in graded-index multimode fibres," *Nat. Commun.* **4**(1), 1719 (2013).
18. K. Krupa, A. Tonello, B. M. Shalaby, M. Fabert, A. Barthélémy, and G. Millot, S. Wabnitz, and V. Couderc, "Spatial beam self-cleaning in multimode fibre," *Nat. Photonics* **11**(4), 237–241 (2017).
19. K. Krupa, A. Tonello, A. Barthélémy, T. Mansuryan, V. Couderc, G. Millot, P. Grellu, D. Modotto, S. A. Babin, and S. Wabnitz, "Multimode nonlinear fiber optics, a spatiotemporal avenue," *APL Photonics* **4**(11), 110901 (2019).
20. T. Hansson, A. Tonello, T. Mansuryan, F. Mangini, M. Zitelli, M. Ferraro, A. Niang, R. Crescenzi, S. Wabnitz, and V. Couderc, "Nonlinear beam self-imaging and self-focusing dynamics in a GRIN multimode optical fiber: theory and experiments," *Opt. Express* **28**(16), 24005–24021 (2020).
21. K. Krupa, A. Tonello, V. Couderc, A. Barthélémy, G. Millot, D. Modotto, and S. Wabnitz, "Spatiotemporal light-beam compression from nonlinear mode coupling," *Phys. Rev. A* **97**(4), 043836 (2018).
22. G. L. Galmiche, Z. S. Eznaveh, M. A. Eftekhari, J. A. Lopez, L. G. Wright, F. Wise, D. Christodoulides, and R. A. Correa, "Visible supercontinuum generation in a graded index multimode fiber pumped at 1064 nm," *Opt. Lett.* **41**(11), 2553–2556 (2016).

23. K. Krupa, C. Louot, V. Couderc, M. Fabert, R. Guenard, B. M. Shalaby, A. Tonello, D. Pagnoux, P. Leproux, A. Bendahmane, R. Dupiol, G. Millot, and S. Wabnitz, "Spatiotemporal characterization of supercontinuum extending from the visible to the midinfrared in a multimode graded-index optical fiber," *Opt. Lett.* **41**(24), 5785–5788 (2016).
24. D. Ceoldo, K. Krupa, A. Tonello, V. Couderc, D. Modotto, U. Minoni, G. Millot, and S. Wabnitz, "Second harmonic generation in multimode graded-index fibers: spatial beam cleaning and multiple harmonic sideband generation," *Opt. Lett.* **42**(5), 971–974 (2017).
25. M. A. Eftekhari, Z. Sanjabi-Eznaveh, J. E. Antonio-Lopez, F. W. Wise, D. N. Christodoulides, and R. Amezcua-Correa, "Instant and efficient second-harmonic generation and downconversion in unprepared graded-index multimode fibers," *Opt. Lett.* **42**(17), 3478–3481 (2017).
26. N. Ould Moussa, T. Mansuryan, C-H Hage, M. Fabert, K. Krupa, A. Tonello, M. Ferraro, L. Leggio, M. Zitelli, F. Mangini, A. Niang, G. Millot, M. Papi, S. Wabnitz, and V. Couderc, "Spatiotemporal beam self-cleaning for high-resolution nonlinear fluorescence imaging with multimode fiber," *Sci. Rep.* **11**(1), 18240 (2021).
27. F. O. Wu, A. U. Hassan, and D. N. Christodoulides, "Thermodynamic theory of highly multimoded nonlinear optical systems," *Nat. Photonics* **13**(11), 776–782 (2019).
28. A. Fusaro, J. Garnier, K. Krupa, G. Millot, and A. Picozzi, "Dramatic acceleration of wave condensation mediated by disorder in multimode fibers," *Phys. Rev. Lett.* **122**(12), 123902 (2019).
29. P. Aschieri, J. Garnier, C. Michel, V. Doya, and A. Picozzi, "Condensation and thermalization of classical optical waves in a waveguide," *Phys. Rev. A* **83**(3), 033838 (2011).
30. E V Podivilov, D S Kharenko, V A Gonta, K. Krupa, O S Sidelnikov, S. Turitsyn, M P Fedoruk, S A Babin, and S. Wabnitz, "Hydrodynamic 2D Turbulence and Spatial Beam Condensation in Multimode Optical Fibers," *Phys. Rev. Lett.* **122**(10), 103902 (2019).
31. T. Shimanouchi, "Tables of molecular vibrational frequencies. Consolidated volume II," *J. Phys. Chem. Ref. Data* **6**(3), 993–1102 (1977).
32. E. O. Faoláin, M. B. Hunter, J. M. Byrne, P. Kelehan, H. A. Lambkin, H. J. Byrne, and F. M. Lyng, "Raman spectroscopic evaluation of efficacy of current paraffin wax section dewaxing agents," *J Histochem Cytochem.* **53**(1), 121–129 (2005).